Research Square

Preprints are preliminary reports that have not undergone peer review.
They should not be considered conclusive, used to inform clinical practice,
or referenced by the media as validated information.

Quantitative time-embedded 3D ECG: two-lead waveform segmentation and timing

Alejandro Jesús Bermejo Valdés

ajbermejo@riojasalud.es

Hospital San Millan-San Pedro De La Rioja: Hospital San Pedro https://orcid.org/0000-0002-8407-487X

Jessica Archer Jiménez

Hospital San Pedro https://orcid.org/0000-0002-6196-102X

Research Article

Keywords: 3D ECG, Vectorcardiography, ECG segmentation, Wave delineation, Causal processing

Posted Date: November 24th, 2026

DOI: https://doi.org/10.21203/rs.3.rs-11829247/v1

License: This work is licensed under a Creative Commons Attribution 4.0 International License.
Read Full License

Additional Declarations: The authors declare no competing interests.

Quantitative time-embedded 3D ECG: two-lead waveform segmentation and timing

Alejandro Jesús Bermejo Valdés[1*] and Jessica Archer Jiménez[1]

[1*]061 Emergency Medical Services Department, La Rioja Health Service, Calle Piqueras 98, Logroño, 26006, Spain.

*Corresponding author(s). E-mail(s): ajbermejo@riojasalud.es;

Abstract

Purpose: To develop and evaluate a quantitative extension of time-embedded 3D ECG for automated waveform segmentation and timing from V1 and V6.

Methods: LUDB provided 619 complete development cycles from 98 patients and 427 evaluation cycles from 70 patients. Joint V1/V6 descriptors were compared with voltage-only, additive, explicit curvature/turning, reconstructed vectorcardiographic and eight-lead dictionaries. Patient-separated selection supported P/QRS/T segmentation within qualified cycle masks, interlead timing and bounded-lookahead processing. Inference used no annotation-derived candidates. The historically examined partition was treated as exploratory, with 453 secondary comparisons.

Results: Joint descriptors achieved 89.97% macro-Dice versus 81.96% for voltages alone. Interlead timing loss decreased from 39.15 to 23.59 ms, and lookahead-integrated QRS-offset loss from 20.17 to 11.81 ms (all adjusted $\boldsymbol{P < 0.001}$). Additive and Kors macro-Dice were 89.79% and 90.86%; explicit curvature/turning achieved 86.88%. Independent calculations reproduced predictions and inference, including 1050 causality checks.

Conclusion: Joint V1/V6 descriptors provide a computational measurement layer for time-embedded 3D ECG, supporting whole-wave segmentation and timing from two leads. The demonstrated benefit is improved performance over the tested voltage-only model; additive and vectorcardiographic controls define its scope.

Keywords: 3D ECG, Vectorcardiography, ECG segmentation, LUDB, Wave delineation, Causal processing

1 Introduction

Time-embedded 3D ECG represents V1, V6 and time as a trajectory [1]. Their temporal correspondence permits quantitative descriptions of joint variation and waveform measurements alongside the visual representation.

We evaluate that application through three tasks: sample-wise P/QRS/T segmentation, V1–V6 onset/offset relationships and QRS delimitation under bounded future context. Joint voltage and difference descriptors are distinguished from explicit curvature/turning operators. Conventional voltage and additive controls assess the value of descriptor construction; Kors and inverse-Dower reconstructions provide established vectorcardiographic comparators [2, 3] (Fig. 1).

Multilead delineation, two-lead timing and trajectory geometry have precedents [4–6]. The contribution here is their operational evaluation within the time-embedded 3D ECG framework, using manual LUDB references [7–9] and reproducible temporal constraints. Kors-derived processing on LUDB has precedent [10].

2 Methods

2.1 Data and reference construction

LUDB 1.0.1 contains 200 ten-second, 500-Hz, 12-lead recordings. We reused the historical 120/80 development/evaluation partition from reconstruction research [11]. Previous examination of this partition makes the present analyses exploratory. Amendments were fixed before their own calculations, after earlier outcomes.

Inputs preserve stored digital-amplitude ratios before representation normalisation. Header gains equal digital ranges; header conversion changes interlead weighting without resolving physical calibration. Derived vectorcardiograms (VCGs) are stored-scale comparators; their physical fidelity remains unverified. Kors/inverse-Dower matrices use $(V1, \ldots, V6, I, II)$.

QRS triplets were reciprocally associated to V3 within 100 ms across leads. Qualified cycles require complete P/QRS/T triplets in all twelve leads and chronologically separated global supports, spanning earliest onset to latest offset. P onset must be at least 1 s and T offset precede 9.6 s. Extra annotated peaks or overlapping cycles invalidate a span. Consecutive accepted cycles are bridged only when no additional waveform peak occurs in any lead. The resulting operational mask includes inferred background; other regions remain unknown. No marks were transferred between beats (Online Resource 9).

2.2 Quantitative 3D ECG implementation

Each method classifies every 2-ms sample without annotation-derived candidates or windows. A causal running mean with 1-s time constant, first-order 20-Hz low-pass and recursive representation root-mean-square normalisation provide the front-end. Initial conditions are specified in Online Resource 9.

For the time-embedded trajectory $r(t) = (u_1, u_6, t/\tau)$, $\tau = 100$ ms, joint descriptors use its V1–V6 voltage projection. The dictionary appends four traces: Euclidean magnitudes of voltage, first and second backward differences, and adjacent-difference

dot products. The additive control replaces the three magnitudes by sums of component absolute values. Explicit curvature/turning instead uses the full trajectory r. Differences use 20-ms backward steps. Voltage-only V1/V6, Kors, inverse Dower and ECG8 complete the seven dictionaries; VCG/ECG8 append the same four joint summaries in their respective dimensions.

Fifteen context offsets span −400 to +400 ms for the main segmentation. Joint, additive, curvature/turning, voltage-only, Kors, inverse-Dower and ECG8 dictionaries contain 90, 90, 60, 30, 105, 105 and 180 columns. Each may select linear ridge or 128-landmark Nyström Gaussian-kernel ridge [12], with five regularisation values. Three development patient folds select by global macro-Dice. Scaling, bandwidth and landmarks are fold-specific. Training samples a fixed 10-ms grid within development masks, weighting patients equally and their four global classes equally. Twelve one-hot outputs encode global, V1 and V6 background/P/QRS/T heads; each uses argmax.

2.3 Segmentation and temporal endpoints

Segmentation loss is one minus patient-mean macro-Dice across P/QRS/T within the mask, using 400-ms lookahead. Intersection over union (IoU), component recovery and boundary errors are retained. Maximal predicted components are extracted on the full record. One-to-one maximum-IoU assignment matches references for evaluation, requiring IoU at least 0.1. Unmatched components wholly within the known mask count as conditional false components.

The individual-lead heads estimate V1-minus-V6 onset and offset differences. Relationship loss averages six absolute errors per patient, capped at 200 ms, assigning that penalty when either component is missing. Signed bias, uncapped error, pair coverage and overlap-duration error are retained.

Each dictionary is refitted at lookahead $L = 0, 40, 100, 200, 400$ ms by shifting context offsets by $L - 400$ ms. A QRS component closes after five non-QRS samples, bridging shorter gaps. Its estimated offset is the last QRS sample; the algorithmic emission timestamp is 10 ms plus L later, excluding computation time. Components lacking recorded closure/context are rejected. The third endpoint integrates patient-level capped/missing-penalised QRS-offset loss across the lookahead grid, divided by 400 ms. This area measures error; emission delay is reported separately.

2.4 Statistics and reproducibility

Eleven contrasts per endpoint compare joint/curvature dictionaries with specified controls. These 33 tests extend the secondary Holm family from 420 to 453; two original primary augmentation tests retain separate correction. Intervals use 10000 patient bootstraps; two-sided sign-flip tests use one million draws and assume symmetric/exchangeable paired differences. Inference conditions on development fits, with patients as the statistical units.

Online Resources 1–8 preserve preceding fiducial, nonlinear, component, storage-limit and selective-risk analyses [13], including wavelet controls [14], under their original protocols and denominators. Independent reference decoding, recursive features

and singular-value-decomposition fitting checked selection, predictions and statistics. Prefix/suffix tests assessed causality; a fresh execution assessed reproducibility.

3 Results

3.1 Whole-wave segmentation from V1 and V6

Complete-cycle criteria retained 1046 cycles: 619 cycles from 98 development patients and 427 from 70 evaluation patients. Evaluation included 176434 known samples; training used 51110 grid samples.

Joint descriptors achieved 89.97% macro-Dice, compared with 81.96% for voltage-only V1/V6. P, QRS and T Dice were 87.10, 93.23 and 89.58%, respectively (Table 1). Joint-minus-voltage segmentation loss was -8.01 percentage points [-9.71, -6.41], adjusted $P < 0.001$.

Additive, Kors, inverse-Dower and ECG8 macro-Dice were 89.79, 90.86, 90.77 and 91.08%. Joint features did not outperform the additive control; Kors had 0.89-point lower loss ($P = 0.020$). Explicit curvature/turning achieved 86.88%, 3.09 points below joint descriptors ($P < 0.001$). These controls distinguish the useful descriptor dictionary from a general advantage of geometric operators.

Table 1 Complete P–QRS–T segmentation and timing losses

Dictionary	P Dice (%)	QRS Dice (%)	T Dice (%)	Relation (ms)	Area (ms)
Joint V1/V6	87.10	93.23	89.58	23.59	11.81
3D curvature/turning	84.34	92.47	83.83	23.73	15.63
Additive V1/V6	87.36	93.27	88.73	24.42	11.90
V1/V6 voltages	74.23	91.14	80.51	39.15	20.17
Kors	87.68	93.62	91.27	21.33	10.90
Inverse Dower	87.57	93.63	91.10	20.73	10.70
ECG8	88.18	93.65	91.42	20.77	10.55

All metrics give equal weight to 70 patients (427 qualified cycles). Dice scores the operational annotation mask, using 400-ms lookahead. Relation averages six V1-minus-V6 onset/offset errors, capped at 200 ms with that penalty for missing pairs. Area integrates failure-aware QRS-offset loss over 0–400-ms lookahead; it is not emission delay. These are conditional internal results, not whole-record diagnostic performance.

3.2 Interlead timing and temporal constraints

Joint-feature relationship loss was 23.59 ms versus 39.15 ms for voltages alone, a difference of -15.56 ms [-22.15, -9.71], adjusted $P < 0.001$. Corresponding additive and Kors losses were 24.42 and 21.33 ms.

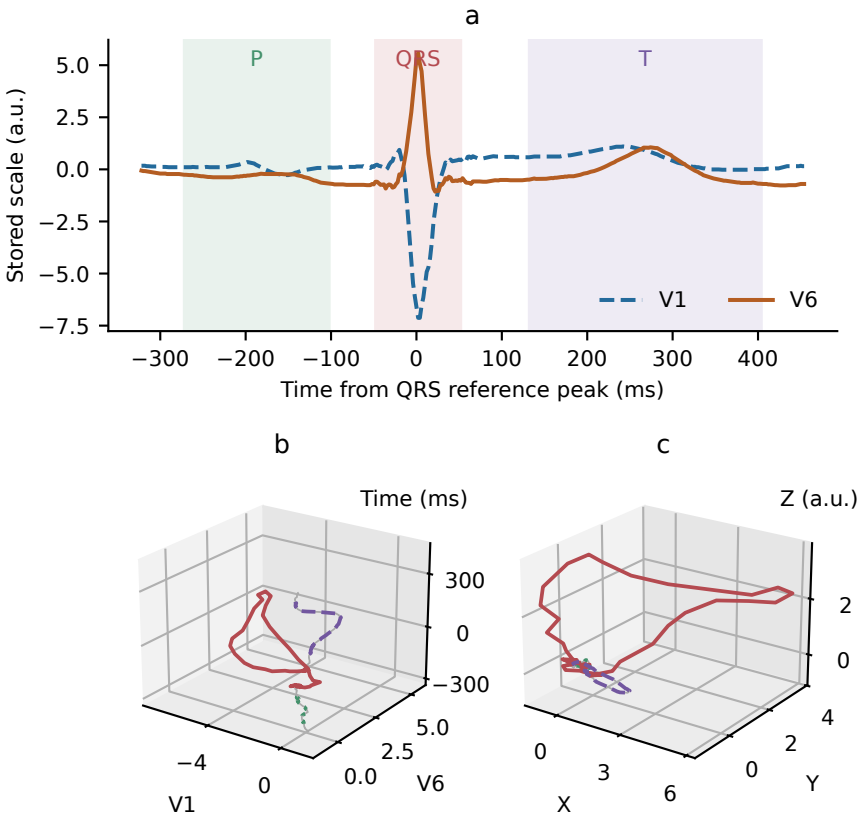

Fig. 1 Representations of LUDB record 2, cycle 1, selected by the lowest qualified evaluation identifier. **a** Conventional V1/V6 inputs. **b** Time-embedded 3D ECG. **c** Kors-derived VCG. Dotted, solid and dashed trajectories identify P/QRS/T supports. Voltage axes use the stored digital scale after common display normalisation. Signals are centred for illustration; model preprocessing is specified in Methods

Lookahead-integrated QRS-offset loss decreased from 20.17 ms for voltages to 11.81 ms for joint descriptors: difference -8.36 ms [-11.14, -6.09], adjusted $P < 0.001$. Additive and Kors losses were 11.90 and 10.90 ms; joint superiority over these controls was not established (Table 2).

Without future context, joint loss was 14.43 ms with algorithmic emission delay 22 ms (median of patient medians); at 400-ms lookahead, loss was 10.20 ms and delay 413.5 ms. All fixed lookahead values are shown in Fig. 2. Curvature/turning at 40 ms produced a median delay of -2 ms with 42.60-ms loss, illustrating the need to assess delay alongside accuracy.

Table 2 Selected paired patient-loss differences

Contrast	Difference	95% CI	Adjusted P
Joint–voltages: segmentation (pp)	-8.01	[-9.71, -6.41]	< 0.001
Joint–voltages: relationships (ms)	-15.56	[-22.15, -9.71]	< 0.001
Joint–voltages: lookahead area (ms)	-8.36	[-11.14, -6.09]	< 0.001
Joint–additive: segmentation (pp)	-0.18	[-0.42, 0.11]	1.000
Joint–additive: relationships (ms)	-0.83	[-1.52, -0.16]	1.000
Joint–additive: lookahead area (ms)	-0.09	[-0.46, 0.47]	1.000
Joint–Kors: segmentation (pp)	0.89	[0.43, 1.49]	0.020
3D curvature–joint: segmentation (pp)	3.09	[2.15, 3.98]	< 0.001

Negative differences favour the first method. Segmentation loss is one minus macro-Dice; pp denotes percentage points. All rows use Holm453. Pointwise intervals condition on development fits and are not simultaneous intervals. Resource 9 reports all 33 new contrasts, including adverse results; the two original primary hypotheses retain separate Holm2 correction.

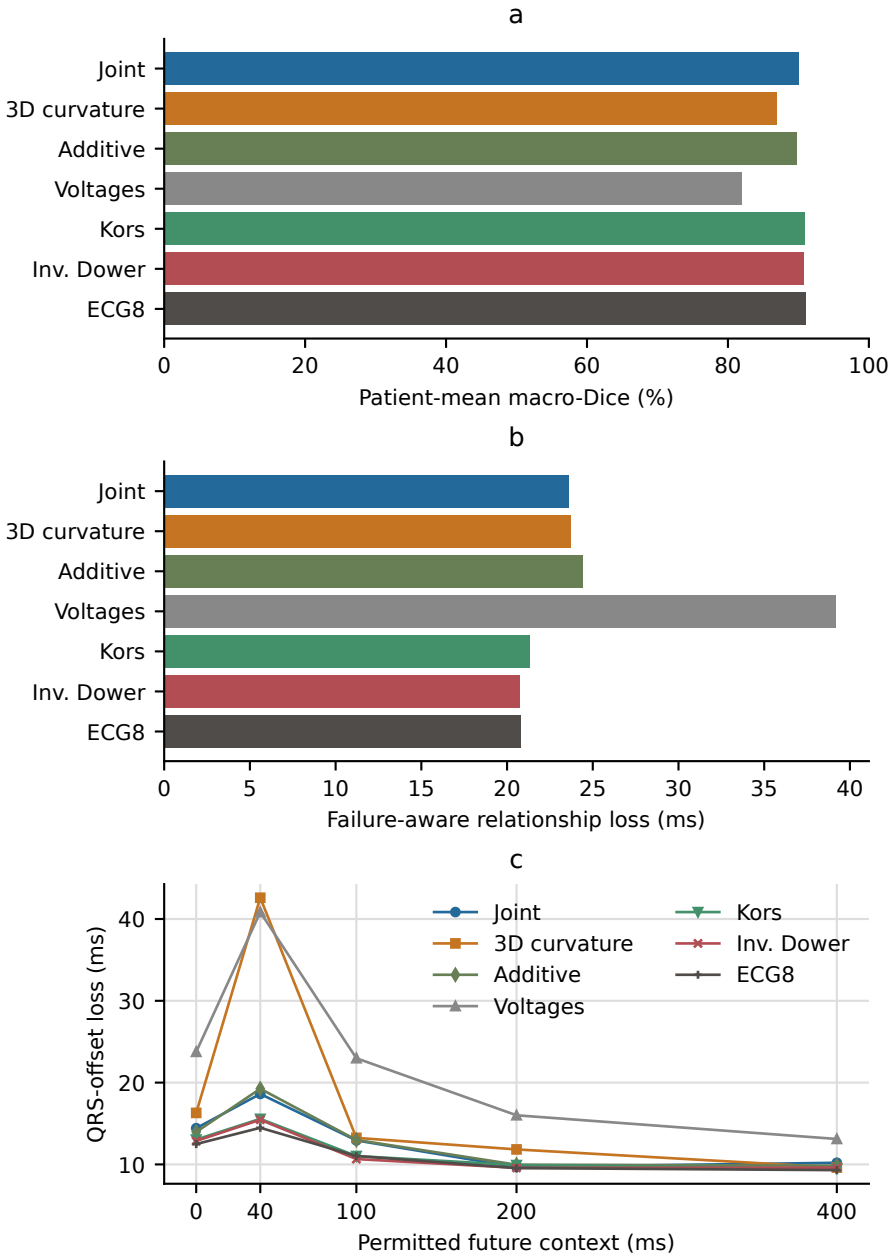

Fig. 2 Patient-weighted results for 70 evaluation patients. **a** P/QRS/T macro-Dice with 400-ms lookahead. **b** V1-minus-V6 onset/offset loss. **c** QRS-offset loss across the complete lookahead grid. Higher Dice and lower losses are favourable. Timing losses penalise missing outputs and cap errors at 200 ms; panel c shows error, not emission delay

3.3 Implementation verification and preceding analyses

Independent calculations reproduced 35 selected models, 42 million full-record labels across all 80 evaluation recordings, and all 33 new contrasts. Maximum score discrepancy was 5.9×10^{-11} without label disagreements. All 1050 causality tests passed. Clean execution reproduced 1472 array files, 20 tables and one structured output, excluding fitting duration.

Earlier candidate-based models also provided compact implementations: joint-feature QRS-offset loss was 9.45 ms versus 12.70 ms for voltages under an 8-KiB prediction-array budget. Those results concern 706 complexes from 79 evaluation patients (Online Resource 8). Original primary VCG-augmentation contrasts remained negative (+0.27/+0.41 ms; both Holm2 $P = 0.622$). Complete preceding results, including adverse noise sensitivities, remain available with current secondary correction.

4 Discussion

The study develops time-embedded 3D ECG into an executable measurement framework using V1 and V6. Its demonstrated utility is the joint descriptor dictionary: the same two acquired signals support more accurate segmentation and temporal estimates than the tested voltage-only model. The 8.01-point macro-Dice improvement extends the quantitative application across P, QRS and T.

The interlead task adds an explicit measurement of how V1 and V6 boundaries relate in time. Individual-lead outputs alongside global support make lead-dependent timing inspectable and reproducible. The measurements concern annotation timing, not physiological dispersion.

The temporal experiment specifies and tests permissible future context and algorithmic emission timestamps. This permits an accuracy–delay comparison without treating computation time as measurement latency. Together with the compact-model results, this supports a reproducible two-lead implementation.

The contribution is this evaluated implementation and its reproducible measurement protocol. Additive features retained similar performance, and reconstructed VCGs were competitive; the results therefore support the joint dictionary rather than exclusive benefit from three-dimensional display or curvature. VCG/ECG8 use eight input leads against two for V1/V6, while global references aggregate twelve.

Limitations include the repeatedly examined LUDB partition, selective complete-cycle eligibility, inferred background and global references, unresolved physical calibration, unequal effective model capacity and one landmark seed. Multiplicity correction does not remove historical reuse. The work is an internal engineering evaluation rather than an external or state-of-the-art benchmark [15]. Reader efficiency, clinical diagnoses and measurement agreement with directly recorded Frank signals were not evaluated.

5 Conclusion

Joint V1/V6 descriptors provide a quantitative extension of time-embedded 3D ECG for whole-wave segmentation, interlead timing and processing with bounded lookahead. Their improvement over the tested voltage-only model supports this two-lead signal-processing application within the exploratory LUDB evaluation, with independently reproduced calculations and an openly reproducible protocol.

Supplementary information

Online Resources 1–9 are deposited in Mendeley Data, version 1 [16], at https://doi.org/10.17632/s2cvjg4tzw.1.

Online Resource 1: reference construction and original protocol. Online Resource 2: complete original results and updated comparisons. Online Resource 3: analysis code, models, derived data, predictions and reproduction instructions. Online Resource 4: numerical verification. Online Resource 5: measurement inventory. Online Resource 6: nonlinear and candidate controls. Online Resource 7: learning, component and explicit-geometry analyses. Online Resource 8: storage limits and selective risk. Online Resource 9: dense segmentation, interlead timing, bounded-lookahead results and all 33 new contrasts.

References

[1] Bermejo Valdés, A. J. (2025). Three-dimensional standard electrocardiogram: a first approach based on precordial leads. *Journal of Electrocardiology, 89*, 153875. https://doi.org/10.1016/j.jelectrocard.2025.153875

[2] Kors, J. A., van Herpen, G., Sittig, A. C., & van Bemmel, J. H. (1990). Reconstruction of the Frank vectorcardiogram from standard electrocardiographic leads: diagnostic comparison of different methods. *European Heart Journal, 11*, 1083–1092. https://doi.org/10.1093/oxfordjournals.eurheartj.a059647

[3] Edenbrandt, L., & Pahlm, O. (1988). Vectorcardiogram synthesized from a 12-lead ECG: superiority of the inverse Dower matrix. *Journal of Electrocardiology, 21*, 361–367. https://doi.org/10.1016/0022-0736(88)90113-6

[4] Almeida, R., Martínez, J. P., Rocha, A. P., & Laguna, P. (2009). Multilead ECG delineation using spatially projected leads from wavelet transform loops. *IEEE Transactions on Biomedical Engineering, 56*, 1996–2005. https://doi.org/10.1109/TBME.2009.2021658

[5] Almeida, R., Martínez, J. P., Rocha, A. P., & Laguna, P. (2009). Are 2 electrocardiographic leads enough for multilead wave boundary location and QT measuring? *Computers in Cardiology, 36*, 593–596. https://diec.unizar.es/~laguna/personal/publicaciones/cinc09almeida.pdf

[6] Yang, H., Bukkapatnam, S. T. S., & Komanduri, R. (2012). Spatiotemporal representation of cardiac vectorcardiogram (VCG) signals. *BioMedical Engineering OnLine, 11*, 16. https://doi.org/10.1186/1475-925X-11-16

[7] Kalyakulina, A., Yusipov, I., Moskalenko, V., et al. (2021). Lobachevsky University Electrocardiography Database (version 1.0.1). *PhysioNet*. https://doi.org/10.13026/eegm-h675

[8] Kalyakulina, A. I., Yusipov, I. I., Moskalenko, V. A., et al. (2020). LUDB: A new open-access validation tool for electrocardiogram delineation algorithms. *IEEE Access, 8*, 186181–186190. https://doi.org/10.1109/ACCESS.2020.3029211

[9] Pollard, T., Moody, B. E., Lehman, L., et al. (2026). PhysioNet as a global platform for biomedical research. *Nature Health, 1*, 792–795. https://doi.org/10.1038/s44360-026-00096-z

[10] Mehri, M., Calmon, G., Odille, F., & Oster, J. (2023). A deep learning architecture using 3D vectorcardiogram to detect R-peaks in ECG with enhanced precision. *Sensors, 23*, 2288. https://doi.org/10.3390/s23042288

[11] Bermejo Valdés, A. J., & Archer Jiménez, J. (2026). Reconstructing the range-normalized terminal QRS from V1 and V6 using the time-embedded 3D ECG. *medRxiv* [Preprint]. https://doi.org/10.64898/2026.11.14.26368083

[12] Williams, C. K. I., & Seeger, M. (2001). Using the Nyström method to speed up kernel machines. *Advances in Neural Information Processing Systems, 13*, 682–688. https://papers.nips.cc/paper/2000/file/19de10adbaa1b2ee13f77f679fa1483a-Paper.pdf

[13] Geifman, Y., & El-Yaniv, R. (2019). SelectiveNet: A deep neural network with an integrated reject option. *Proceedings of Machine Learning Research, 97*, 2151–2159. https://proceedings.mlr.press/v97/geifman19a.html

[14] Makowski, D., Pham, T., Lau, Z. J., et al. (2021). NeuroKit2: a Python toolbox for neurophysiological signal processing. *Behavior Research Methods, 53*, 1689–1696. https://doi.org/10.3758/s13428-020-01516-y

[15] Joung, C., Kim, M., Paik, T., et al. (2024). Deep learning based ECG segmentation for delineation of diverse arrhythmias. *PLOS ONE, 19*, e0303178. https://doi.org/10.1371/journal.pone.0303178

[16] Bermejo Valdés, A. J. (2026). Quantitative time-embedded 3D ECG: two-lead waveform segmentation and timing. Supplementary data and code (Version 1). *Mendeley Data*. https://doi.org/10.17632/s2cvjg4tzw.1

Statements and Declarations

Funding. No external funding.

Competing interests. No competing financial interests or personal relationships. Non-financial interests: the authors have developed and published related 3D ECG work.

Ethics approval. No additional approval was sought for secondary analysis of public, de-identified recordings. There was no recruitment, contact, intervention, access to personal identifiers or re-identification keys, or new personal-data collection. LUDB documents original institutional approval (No. 23, 19 October 2017).

Consent to participate and publish. No new consent was obtained for this secondary analysis. LUDB documents original consent; this study used publicly released, de-identified recordings and repository identifiers.

Author contributions. Alejandro Jesús Bermejo Valdés: Conceptualization, Methodology, Software, Validation, Formal analysis, Investigation, Resources, Data Curation, Writing – Original Draft, Writing – Review and Editing, Visualization, Supervision, Project administration. Jessica Archer Jiménez: Conceptualization, Methodology, Investigation, Writing – Original Draft, Writing – Review and Editing, Visualization, Supervision.

Data and code availability. The code, models, derived data, results and supplementary documents are deposited in Mendeley Data, version 1 [16], at https://doi.org/10.17632/s2cvjg4tzw.1.